AGU
ADVANCING EARTH AND SPACE SCIENCE

Tectonics®

Key Points:

- Paleoseismological characterization of the longest crustal seismic fault system near Mexico City
- New stratigraphic evidence of two paleoearthquakes along the Venta de Bravo Fault in the Acambay Graben
- New evidence of possible seismic rupture coalescence associated with an $M > 7$ earthquake in the densely populated Central Mexico

Correspondence to:
P. Lacan,
placan@geociencias.unam.mx

Paleoseismology of a Major Crustal Seismogenic Source Near Mexico City: The Southern Border of the Acambay Graben

Rodrigo León-Loya[1] [ID], **Pierre Lacan[2]** [ID], **María Ortuño[3]**, **F. Ramón Zúñiga[2]** [ID], **Petra Štěpančíková[4]** [ID], **Jakub Stemberk[4]** [ID], **Ana Paula Hernández Flores[5]**, **Jaime J. Carrera Hernández[2]** [ID], **Ivan Sunyé-Puchol[1,6]**, **Gerardo J. Aguirre-Díaz[2]**, and **Laurence Audin[7]** [ID]

[1]Posgrado en Ciencias de la Tierra, Centro de Geociencias, Universidad Nacional Autónoma de México, Juriquilla, México, [2]Centro de Geociencias, Universidad Nacional Autónoma de México, Juriquilla, México, [3]Earth and Ocean Dynamics Department, RISKNAT Group, Geomodels Institute, Universitat de Barcelona, Barcelona, Spain, [4]Department of Neotectonics and Thermochronology, Institute of Rock Structure and Mechanics, Czech Academy of Sciences, Prague, Czech Republic, [5]Departamento de Geología, Centro de Investigación Científica y de Educación Superior de Ensenada, Ensenada, México, [6]Department of Earth Sciences, Sapienza University of Rome, Roma, Italy, [7]Institut des Sciences de la Terre, ISTerre, IRD, Université Grenoble Alpes, Grenoble, France

Abstract The Trans-Mexican Volcanic Belt is an active continental volcanic arc related to subduction along the Middle America trench. It is characterized by intra-arc extension resulting into several major arc-parallel active fault systems and tectonic basins. The Acambay graben, one of the largest of these basins, is located near Mexico City, in the central part of this province. In 1912, a M 6.9 earthquake ruptured the surface along the northern border of the graben together with at least two other faults. In this paper, we analyze the paleoseismic history of the southern border of the Acambay Graben, with new observations made in one natural outcrop and four paleoseismological trenches excavated across branches of the Venta de Bravo Fault at the site where it overlaps with the Pastores Fault. We present evidence of at least two paleo-earthquakes that occurred between $12,190 \pm 175$ and $5,822 \pm 87$ cal year BP and between 647 ± 77 and 250 cal year BP. On one of these branches, we estimate a minimum slip-rate value between 0.1 and 0.23 mm/year for the last 12 ka and a mean recurrence interval of 8.5 ± 3 ka. By considering several likely rupture lengths along the Venta de Bravo and Pastores faults, we calculated a maximum possible magnitude of $M_w\ 7.01 \pm 0.27$. Finally, by correlating events recorded along different faults within the Acambay Graben, we discuss several possible rupture coalescent scenarios and related consequences for Mexico City.

Plain Language Summary The Trans-Mexican Volcanic arc is affected by several fault systems. Activity on these faults results in an extension of the crust and the formation of elongated topographic depressions. The study region, called the Acambay Graben, is one of these depressions and is bounded by normal E-W active faults. In 1912 an M 6.9 earthquake caused nearly 300 fatalities and generated a surface rupture along three faults which are the boundaries of this depression. The epicenter of this event is in a region where close to 24 million inhabitants are living; therefore, the history of past earthquakes is crucial in evaluating the seismic hazard of central Mexico. We conducted paleoseismological excavations on one of these faults, the Venta de Bravo Fault, to infer the record of past earthquakes. The results show that at least two earthquakes occurred in the past: one between 12,365 and 5,735 cal year BP and the other between 724 and 250 cal year BP. With this new data and the previously published, we compiled the paleoseismic catalog for this region and discussed the different possibilities of earthquake surface ruptures implying multiple faults. This new data will help to better understand central Mexico's seismic hazard assessment, especially relevant for Mexico City.

1. Introduction

Continental earthquakes with complex surface ruptures highlight the importance of considering the influence of strike-variable geometries of rupture propagation across neighboring faults for seismic hazard assessment (Biasi & Wesnousky, 2016; Mildon et al., 2016). When the rupture propagates through more than one fault segment, an unexpectedly large magnitude earthquake may be generated (e.g., Biasi & Wesnousky, 2017; Fletcher et al., 2014). Such multi-fault crustal ruptures on normal faults have affected the Mexican territory in historical
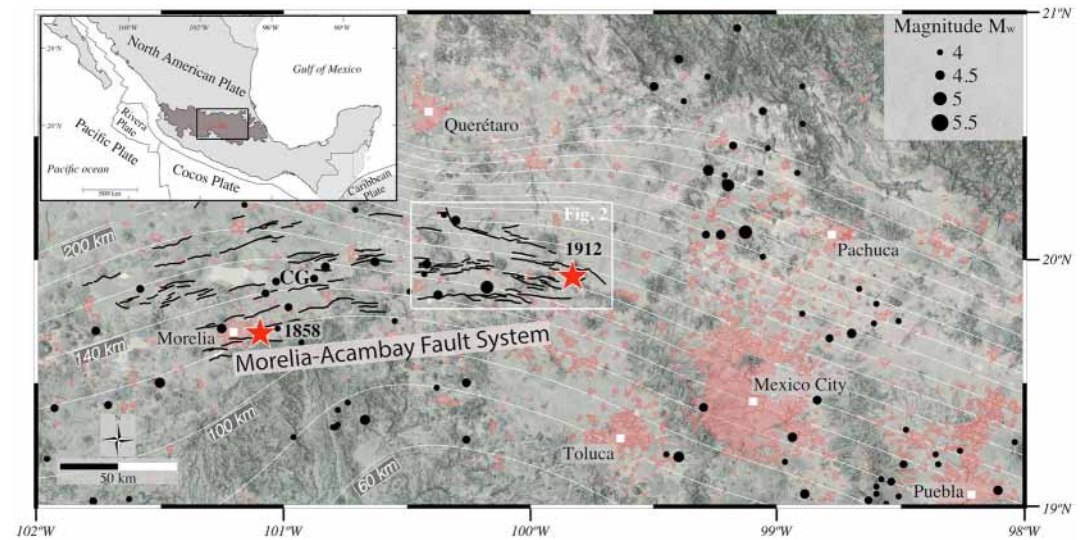
Figure 1. Map of the central part of the Trans-Mexican volcanic Belt. Black lines represent the Morelia-Acambay Fault System, black dots the epicenters from Servicio Sismologico Nacional (SSN, 2022) catalog (M_w > 4.5), red stars the historical earthquakes (Suárez et al., 2019; Suter et al., 1996). Solid white lines are representing the isodepth of the top of the Cocos slab beneath the North American plate (Hayes, 2018). White squares are the location of major cities and red polygons are the urban areas (CONABIO, 2015). CG, Cuitzeo Graben.

and recent times and need to be considered for a better evaluation of the seismic hazard of the region (e.g., the 1567–1568 Ameca M_w 7.2 earthquake; Núñez-Meneses et al., 2021; Suárez et al., 1994; Suter, 2015a, 2019; the 1887 Pitáycachi M_w 7.5 earthquake; Suter, 2008, 2015b; the 1912 Acambay M_w 6.9 earthquake; Abe, 1981; Urbina & Camacho, 1913; and El Mayor-Cucapah *Mw* 7.2 2010 earthquake; Fletcher et al., 2014, 2020; Wei et al., 2011).

In Mexico, most of the population is concentrated in megacities located in the Trans-Mexican Volcanic Belt (TMVB), a continental volcanic arc that crosses the country from the Pacific coast to the Gulf of Mexico (Figure 1; Ferrari et al., 2012). The seismicity in the central TMVB is described as mostly shallow (<20 km) with a low frequency of occurrence of moderate magnitude events. The instrumental catalog from the Mexican National Seismological Service is complete in the region only for M_c = 4.6 since 1988 (Zúñiga et al., 2020). Nevertheless, intra-arc fault systems in the TMVB are responsible for several major crustal earthquakes in historical times (Suárez et al., 2019, 2020). At least seven M_w > 6 crustal earthquakes have been reported in the last four centuries in the TMVB, two of them taking place within the Morelia Acambay Fault system (MAFS), justifying new studies for a better evaluation of the seismic hazard (Figure 1). The last major earthquake occurred in 1912 in the Acambay Graben (M_w 6.9; Urbina & Camacho, 1913), located 80 km northeast of Mexico City. During this earthquake, three main synthetic and antithetic faults of the graben separated by 5–7 km steps ruptured with associated decimetric displacement (Figure 2, De Mountessus De Ballore, 1913; Lacan & Arango-Galván, 2021; Suter et al., 1996; Urbina & Camacho, 1913).

In this paper we focus on the 80 km long southern border of the Acambay Graben, and introduce new observations made in four paleoseismological trenches excavated at the relay zone between the two main faults bordering the graben to the south: the Venta de Bravo and the Pastores faults. In the light of these new results and previously published paleoseismological data, we discuss the maximum magnitude based on the probable rupture length of paleoearthquakes to infer possible occurrences of a multi-fault rupture along the tectonic structures that form the Acambay Graben.

2. Geological and Neotectonic Setting

2.1. The Trans-Mexican Volcanic Belt (TMVB)

The TMVB is a continental volcanic arc related to the subduction of the Rivera and Cocos plates under the North America plate characterized by a N-S intra-arc extension (setting map of Figure 1; Ferrari et al., 2012;
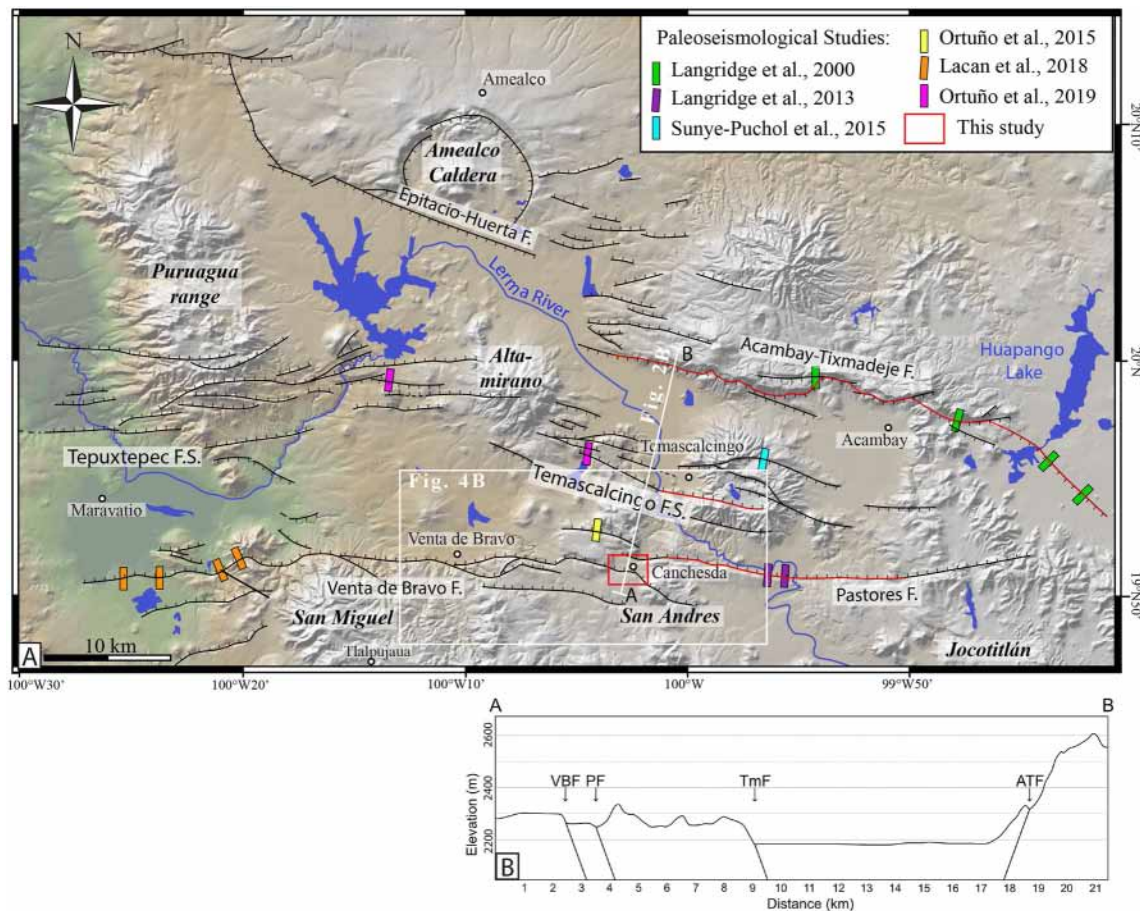
Figure 2. (a) Seismotectonic map of the Acambay Graben. The red lines represent the surface rupture of the 1912 earthquake (After Langridge et al., 2000). Solid black lines depict the active fault traces, modified after Lacan et al. (2018). (b) Topographic profile across the Acambay Graben (derived from GeoMapApp). VBF, Venta de Bravo Fault; PF, Pastores Fault; TmF, Temascalcingo Fault; ATF, Acambay-Tixmadeje Fault.

Gómez-Tuena et al., 2007). This arc can be divided into three sectors by considering the crustal thickness, faulting style, and magmatic composition: the western, central and eastern TMVB (Ferrari et al., 2012). The central TMVB is located between longitudes −102°W to −98°W (Figure 1) and is characterized by a wide variety of Miocene to Quaternary volcanism dotted with large calderas, andesitic stratovolcanoes, small monogenic basaltic scoria cones and andesitic domes (Ferrari et al., 2012; Gómez-Tuena et al., 2007). The central TMVB is cut out by the MAFS formed by E-W striking normal faults that structure a ∼50 km wide horst and graben belt extending over at least 150 km (Figure 1; Ferrari et al., 1999; Martínez-Reyes & Nieto-Samaniego, 1990; Pasquaré et al., 1988). In the eastern MAFS, the faulting initiated during late Miocene under NW-SE extension and later evolved to an almost N-S extension (Ferrari et al., 1990, 2012; Lacan et al., 2018; Suter et al., 1995).

2.2. The Acambay Graben

The Acambay Graben is one of the major and most continuous tectonic structures of the MAFS (Johnson & Harrison, 1990; Suter et al., 1995). This tectonic depression is 80 km long, 15–30 km wide and extends from the Huapango Lake to the east to the Puruagua range to the West (Figure 2). Further west, the structures of the Acambay Graben disappear to give way to those of the Cuitzeo Graben (Figure 1). The lithology consists of Neogene volcanic rocks deposited over a plutonic and metamorphic basement (Ortuño et al., 2015). Synchronously to its opening, the basin was filled by volcanic deposits and fluvio-lacustrine sediments. The faults bounding the graben correspond to topographic steps that range from 50 to 500 m. To the north, the graben is bounded by the Acambay-Tixmadeje Fault and the Epitacio Huerta Fault. To the south, the basin is delimited by the Pastores Fault (PF) and the Venta de Bravo Fault (VBF) that are separated by a 1 km wide stepover and overlap about 13 km
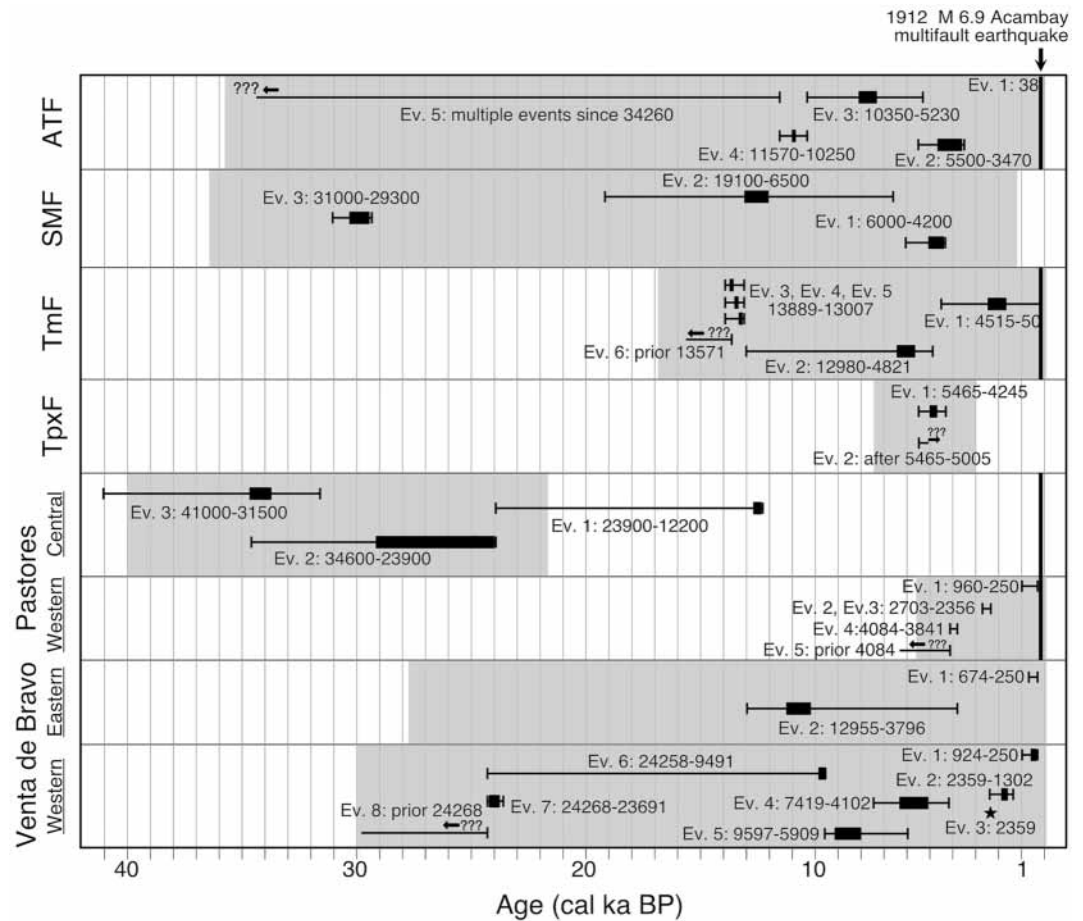
Figure 3. Compilation of paleo earthquakes discovered for the last 40 ka in the Acambay Graben. See Tables 1 and 2 for details. Gray zone: complete sedimentary record within trenches. White zone: incomplete sedimentary record. ATF, Acambay-Tixmadeje Fault; SMF, San Mateo Fault; TemF, Temascalcingo Fault; TepF, Tepuxtepec Fault; PF, Pastores Fault; VBF, Venta de Bravo Fault. Chronology of paleoevents compiled from Lacan et al. (2018), Langridge et al. (2000, 2013), Ortuño et al. (2015, 2019), and Sunye-Puchol et al. (2015). Modified after León-Loya et al. (2022).

(Figure 2, Ortuño et al., 2015). Finally, the center of the graben is faulted by the Temascalcingo-Acámbaro Fault system (TAFS; Martínez-Reyes & Nieto-Samaniego, 1990; Ortuño et al., 2019). This intra-graben fault system cuts the Temascalcingo, Altamirano and Puruagua volcanic edifices (Figure 2, Ortuño et al., 2019; Sunye-Puchol et al., 2015).

In the Acambay graben, at least 31 individual paleo-events with associated surface ruptures have been identified (Figure 3; Lacan et al., 2018; Langridge et al., 2000, 2013; Ortuño et al., 2015, 2019; Sunye-Puchol et al., 2015). They occurred during the last 40 ka with paleoseismic parameters that have been estimated for six of the 10 faults of the graben that exceed 10 km in length. In Table 1, we include a review of the paleoseismological studies to help in discussing the possibility of ruptures along different faults during a single seismic event in the light of new results. The locations of previous studies are shown in Figure 2 and the age constraints of the events are displayed in Figure 3 and Table 2. Paleoseismic parameters such as the slip-rate (from 0.02 to 0.23 mm/year), as well as recurrence intervals (from 1.1 to 11 ka), reflect the variability of completeness of the data and the possibility of stress transfer between structures within the same fault system (León-Loya et al., 2022).

The last surface-rupturing earthquake in the Acambay Graben occurred in 1912. Urbina and Camacho (1913) described in detail the geological effects of this M 6.9 event on different faults of the graben. However, inaccuracies and contradictions between descriptions reported in the text and maps by Urbina and Camacho (1913) resulted in different interpretations of the ruptures and in some controversy within the scientific community (Figure 2, De Mountessus De Ballore, 1913; Lacan & Arango-Galván, 2021; Langridge et al., 2000; Rodríguez-Pascua

Table 1
Compilation of Paleoseismic Parameters From Published Works in the Acambay Graben

	ATF	SMF	TemF	TepF	WPAF	CPAF	WVBF	EVBF
SRL (km)	41	13	19	24	20.4	26	48	48
Number of events	6	3	6	2	5	3	6	2
Recurrence interval (ka)	3.6	5.32–11.57	0.9 (clustered)	not constrain	1.1–2.60	10–14.4	1.94–2.33	10.5
Slip rate (mm/year)	0.17 ± 0.02	0.085 ± 0.025	0.17	0.25 ± 0.01	0.3 ± 0.07	0.03	0.23 ± 0.01	0.1–0.2
SED max/min (cm)	74/46	150/52	75/22	100/25	37/<29	50/<24	100/18	74/52
Mmax (individual fault)	6.8	6.4	6.7	6.5	6.7	6.7	6.9	6.9
Reference	Langridge et al. (2000)	Sunye-Puchol et al. (2015)	Ortuño et al. (2019)	Ortuño et al. (2019)	Ortuño et al. (2015)	Langridge et al. (2013)	Lacan et al. (2018)	This work

Note. The faults that have been studied are: ATF, Acambay-Tixmadejé; SMF, San Mateo; TemF, Temascalcingo; TepF, Tepuxtepec; WPAF, Western Pastores; CPAF, Central Pastores; WVBF, Western Venta de Bravo; EVBF, Eastern Venta de Bravo; SRL, Surface Rupture Length; SED, Single Event Displacement; Mmax, Maximum Magnitude.

et al., 2017; Suter et al., 1996). Most authors agree that the surface rupture and major displacement occurred along the Acambay-Tixmadejé fault, bounding the graben to the north, while other ruptures with a few tens of centimeters of displacement occurred on the PF (bordering the graben to the south) and on the central graben fault system. Most of the controversy concerns the mapping of ruptures along the central graben fault system (e.g., Lacan & Arango-Galván, 2021). However, Langridge et al. (2000) questions also the presence of a rupture along the PF because they could not find any field evidence for a 1912 surface rupture along this fault. In our opinion, this lack of evidence is mostly linked to poor preservation of sedimentary and morphological record of decimetric ruptures on a several hundred meters high fault escarpment and does not necessarily question the post-earthquake observations made by Urbina and Camacho (1913). In any case, despite these few uncertainties on the precise location of rupturing faults, all the authors appear to agree on the fact that different faults, separated by several kilometers, broke together in 1912, causing an earthquake of considerable magnitude.

2.3. The Pastores-Venta de Bravo Fault System

In the last 30 years, several studies on neotectonics and paleoseismology have been performed along the Pastores-Venta de Bravo Fault System (PVBFS), describing the kinematics, geometry, geomorphology and paleoseismicity (Lacan et al., 2018; Langridge et al., 2013; Ortuño et al., 2015; Suter et al., 1992, 1995; Szynkaruk et al., 2004). The fault traces are discontinuous and show multiple overlapping sections. Five fault sections can be distinguished based on (a) orientation of morphological traces, (b) variation of the scarp height along the trace, and (c) presence of relay zones between traces with different degrees of maturity. These fault sections correspond to the eastern and western PF, and the eastern, central and western VBF segments (Figure 4; Lacan et al., 2018; Ortuño et al., 2019).

The PF is 33 km long with a E-W strike and dips 45° to 70° to the north (Arzate et al., 2018). It is expressed by continuous, linear and mostly undissected ~200 m scarps that separate Miocene (to the east) and Pliocene andesitic lavas (to the west) from the Plio-Quaternary infill of the Acambay basin (Figure 4, Langridge et al., 2013; Suter et al., 1995). Paleoseismological studies performed along the central part of the fault show a 10–15 ka recurrence interval of surface faulting and a 0.03 mm/year slip-rate (Langridge et al., 2013). Such slip-rate value is consistent with the estimation of the long-term slip-rate given by Suter et al. (1995) for the easternmost part of the fault (0.04 mm/year). However, the trench site of Langridge et al. (2013) is located relatively high on the slope of the fault escarpment and most of the recent sedimentary record is missing. Thus, younger units are poorly preserved, and the only earthquake recorded after 21.5 ka was interpreted from a fissure filling with an age of 12.2 ka. Consequently, the recurrence interval as well as the slip-rate could have been underestimated. On the contrary, the study performed by Ortuño et al. (2015) on the western splay termination of the fault, near Canchesdá, provides a long-term geological slip-rate of 0.02 mm/year since 3.5 Ma and a Holocene slip-rate of 0.23–0.37 mm/year, with a recurrence interval of 1.1–2.6 ka for surface ruptures based on five possible paleoearthquakes in the last 4 ka. This relatively high recurrence interval over such a short paleoseismological record is interpreted by Ortuño et al. (2015) as potentially overestimated and part of the deformation recorded could be related to a secondary rupture or non-tectonic subsidence. In this context, the slip-rate calculated from evidence from the trench is certainly overestimated.

More to the west, the VBF extends 48 km striking E-W from the San Andrés Volcano to the Cachiví plain and it is divided into different sections that dip 60° to 70° to the North (Figure 4). The fault trace is influenced by the changes in lithology along the strike. The eastern part of the fault lies between Venta de Bravo and the San Andrés volcano, which is formed by five separate traces between 3 and 5 km in length with scarp heights that range from 100 to 200 m overlapping with the western PF (Lacan et al., 2018; Suter et al., 1992). In the central segment, the fault cuts through Miocene to Pliocene volcanic and Cretaceous metamorphic rocks with an associated topographic scarp reaching 350 m. In the western segment, the fault displaces Quaternary lacustrine deposits and dacitic volcanic rocks (Aguirre-Díaz et al., 2000), with a scarp height that

Table 2
Compilation of Paleo-Ruptures Recorded in the Trenches in the Acambay Graben

| Events	Bracketed age (cal year BP)	Preferred age of event
Acambay Tixmadeje Fault (Langridge et al., 2000)		
I	38	Acambay $M = 7$ 1912 earthquake
II	5,500–3,470	Before younger range
III	10,250–5,230	Post 7,965 cal year BP, Organic material in fissure
IV	11,570–10,250	10,770 cal year BP activity of Jocotitlán Volcano
Pre-IV	>34,260	Multiple displacement events
San Mateo Fault (Sunye-Puchol et al., 2015)		
I	6,000–4,200	5,000–4,200
II	19,100–6,500	13,000–12,000
III	31,000–29,300	
Temascalcingo Fault (Ortuño et al., 2019)		
I	4,515–50	
II	12,980–4,821	6.4–5.6 ka
III	13,889–13,007	Clustered events (OxCal age modeling)
IV	13,889–13,007	
V	13,889–13,007	
VI	>13,571	Before deposition of unit with this age range
Tepuxtepec Fault (Ortuño et al., 2019)		
I	5,465–4,245	Possible clustered events
II	<5,465	
Central Pastores Fault (Langridge et al., 2013)		
I	23,900–12,200	12.2–12.6 ka (fissure filled)
II	34,600–23,900	29.1–23.9 ka
III	41,000–31,500	34.6–33.7 ka
Western Pastores Fault (Ortuño et al., 2015)		
I	960–795	1912 earthquake?
II	2,703–2,356	Within the interval
III	2,703–2,356	Shortly after the interval
IV	4,084–3,841	Shortly before the interval
V	>4,084	Undetermined time before age
Western Venta de Bravo Fault (Lacan et al., 2018)		
I	924–250	Historical
II	2,359–1,302	Historical?
III	<2,359	2,359 (Colluvial Wedge)
IV	7,419–4,102	
V	9,597–5,909	6.5–5 kyr
VI	24,268–9,491	<9,737–9,543 years cal BP. Colluvial wedge
VII	<24,268–23,691	
VIII	<24,268	No temporal constrain
Eastern Venta de Bravo Fault (This work)		
I	647–250	Younger than 647 years cal BP
II	12,190–5,822	Closer to older range (12,190 years)
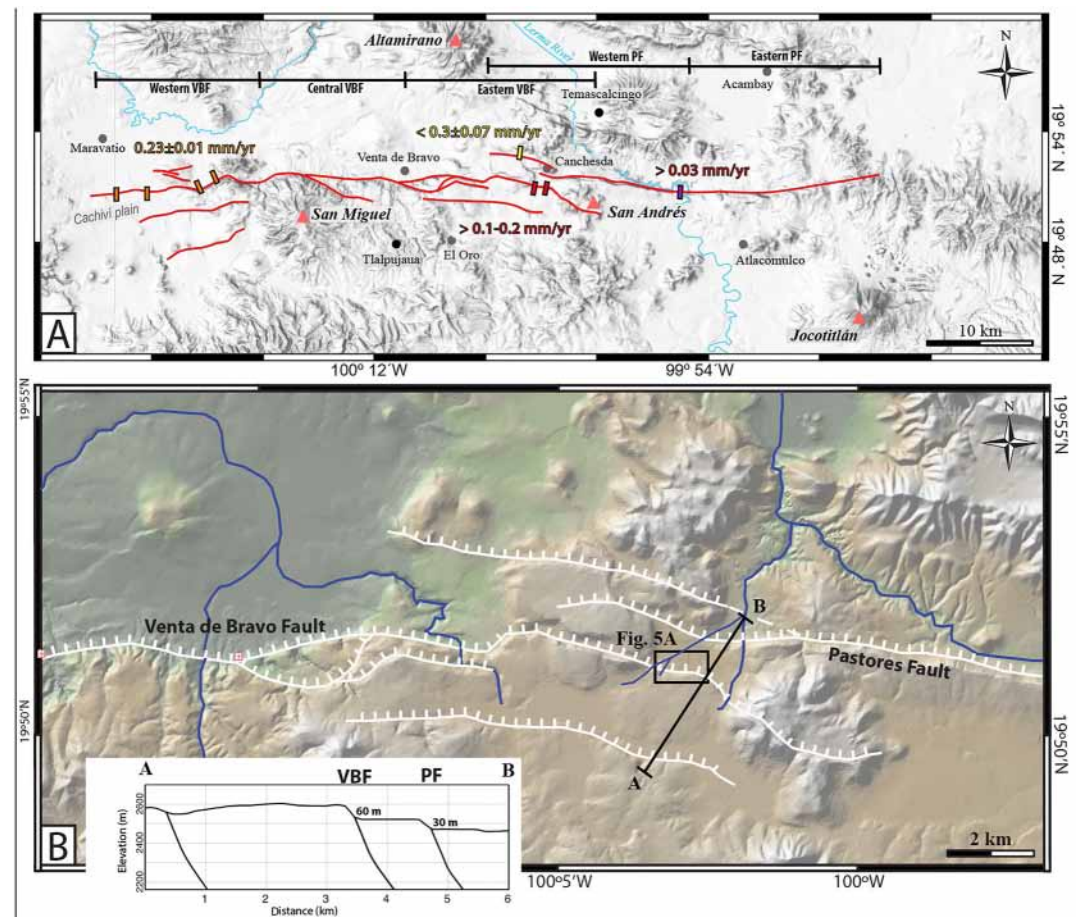
Figure 4. (a) Map of the south border of the Acambay Graben, the Venta de bravo and Pastores faults are represented in red. Colored rectangle correspond to the locations of trench sites of previous studies and the red one represent the location of the Canchesdá trench site. Red triangles represent volcanoes and black dots the principal towns. (b) 30 m resolution digital elevation model and topographic profile across the Pastores-Venta de Bravo Fault System (derived from GeoMapApp).

varies from 50 to 300 m (Lacan et al., 2018). Most of the rocks forming the foot wall are tilted 5° to 10° to the south. The slip-rate for the late Quaternary is estimated at 2 mm/year based on the displacement of lake deposits at the overlap with the PF (Suter et al., 1992). However, this slip-rate, based on the correlation of lacustrine deposits constrained by a single radiocarbon age may be misleading. Indeed, this area contains many discontinuous sub-basins with a complex history and the lake deposits considered displaced could also correspond to deposits of different sub-basins. In this case, this high slip-rate (the highest calculated in the TMVB) could have been overestimated. In this context, the 0.22–0.24 mm/year slip-rate estimated by Lacan et al. (2018) based on the displacements of late Pleistocene to Holocene units by at least eight earthquakes recorded at the western segment seems to be more compatible with the slip-rates calculated at the other faults bordering the graben and could be considered as better representative of the actual slip-rate (Lacan et al., 2018; Langridge et al., 2000).

2.4. Relay Zone Between Pastores Fault (PF) and Venta de Bravo Fault (VBF)

The Pastores and Venta de Bravo faults formed a ~80 km long and ~4 km wide north dipping fault zone divided into five main sections separated by narrow relay zones. This left-stepping *en echelon* array probably resulted from an early stage of the oblique right-lateral extension during Miocene and a dominant normal dip-slip movement during Late Pliocene (Lacan et al., 2018; Suter et al., 1992, 1995).

At the transfer zone between the VBF and PF (Figure 4), a depression between the two faults led Suter et al. (1992) to interpret this area as an extensional jog. At this location, the two faults overlap for about 13 km and are separated by only 1–2.5 km. Recent studies indicate that such a small step-over (<1 km) does not represent an

obstacle for rupture propagation (Biasi & Wesnousky, 2016; Boncio, Lavecchia, & Pace, 2004). It is precisely this area that is the focus of this study.

3. Paleoseismology in the Relay Zone Between Pastores and Venta de Bravo Faults

3.1. Trench Site Selection and Methods

To improve the characterization of the PVBFS, we aimed to complete its paleoseismological record, already studied in the VBF western segment by Lacan et al. (2018) and in the central and eastern PF segments by Langridge et al. (2013) and Ortuño et al. (2015). Therefore, we analyzed the morphology of the fault scarp at the eastern tip of the VBF by satellite images, a 30 m digital elevation model, and a field survey to select the optimal site to trench (Figure 5). The scarp in this area is between 50 and 60 m high, continuous, and transected only by a second-order tributary of the Lerma River. Along the scarp, there are no mappable alluvial terraces or recent fine deposits, but only volcanic fall-out, fluvio-lacustrine and slope deposits filling the depressions formed in the hanging wall of the fault. The observation of a striated bedrock scarp in a nearby creek and the presence of several topographic subtle scarps at the foot of the main scarp led us to choose this area to perform a paleoseismological study (Figure 5). At the creek outcrop, the main trace of the VBF is displacing colluvial deposits showing slickenlines on a bedrock fault plane, developed on andesitic lavas (CanCreek in Table 3). Slickenlines are mainly dip-slip with a minor left-lateral component (Figures 5C and 5D). This free face is partially covered with a thick colluvium that is not suitable for paleoseismological analysis, although it was sampled. Trenching through this main fault branch cutting lavas was not technically possible. However, at the eastern margin of the creek, the base of the scarp presented a marked inflection. A first trench (Canchesdá-4) was excavated there, about 100 m to the east of Canchesdá-creek exposure, it was 4 m deep and 6 m long but had to be closed due to a conflict with the landowners. Because of that drawback, we were able only to take general pictures, field notes and sketches of this trench (Figure 5b-F). Three additional trenches (Canchesda 1, 2 and 3, from east to west, Figure 5a) were excavated further to the east. Canchesdá-1 and Canchesdá-2 were dug at the base of the topographic escarpment, while Canchesdá-3 was dug across a discontinuous 1–2 m high scarp, parallel to the main fault trace and only 40–45 m to the north of it. This small distance indicates that is likely connected at depth with the main fault (Figure 5). Even if these other trenches do not cross the main fault branch, we considered that they could be recording ruptures occurred in more recent fault branches. Fault branches merging at depth with the main fault and located in the hanging wall are widely observed in normal fault ruptures (e.g., Chapter 3 of McCalpin, 2009) and are considered as a migration of the main trace toward the downthrown wall.

For these three last trenches, we used the classical methods of paleoseismological investigation along normal faults (Audemard, 2005; McCalpin, 2009), starting with excavating single-slot trenches with a backhoe machine perpendicularly to the fault. The trenches were 21, 17 and 12 m long respectively, and each has a depth of 2–3 m (Figure 6).

We cleaned both walls of each trench, and a grid of 1×1 m was installed. The exposed faults and units were pinned with color markers, and we proceeded to photograph each part of the grid to construct a photomosaic (Figure 6b). We logged all walls at a 1:10 scale. The samples taken for dating include charcoal and bulk material that were sent for dating by radiocarbon methods (C^{14}) at Beta Analytics Testing Laboratory. The results and details of the samples are reported in Table 4. Ages in the Results section are depicted as conventional ages and in the Discussion section they are presented as calibrated at 2 sigma of confidence level using the OxCal 4.1 program (Bronk Ramsey, 2009).

The value for the maximum possible magnitude is calculated by means of the Wesnousky (2008) Length-Magnitude empirical relationship. This formula was developed for normal faults in extensional environments based on the surface rupture length value (SRL). This relationship is an appropriate choice for the seismotectonic environment of the Acambay Graben active faults. We choose to use this approach rather than estimating the magnitude of the events from the individual displacement recognized, due to the variation of slip along the strike that has been extendedly reported in the literature for normal faults (e.g., Iezzi et al., 2018). The existence of parallel branches, implying a partition of the slip distribution, leads us to consider the record as a minimum slip, thus not suitable for calculating empirical relationships.

3.2. Results

3.2.1. Observations on the Main Fault Scarp

The main fault could be observed in the creek that crossed the VBF at Can-creek station. At this site the fault plane is developed in dacitic lavas corresponding to a part of the Pliocene Bañí dome (Ortuño et al., 2015). The fault plane is oriented ESE-WNW (N98E/58NE N110E/60NE) and contains slickenlines (oriented 53/163) showing
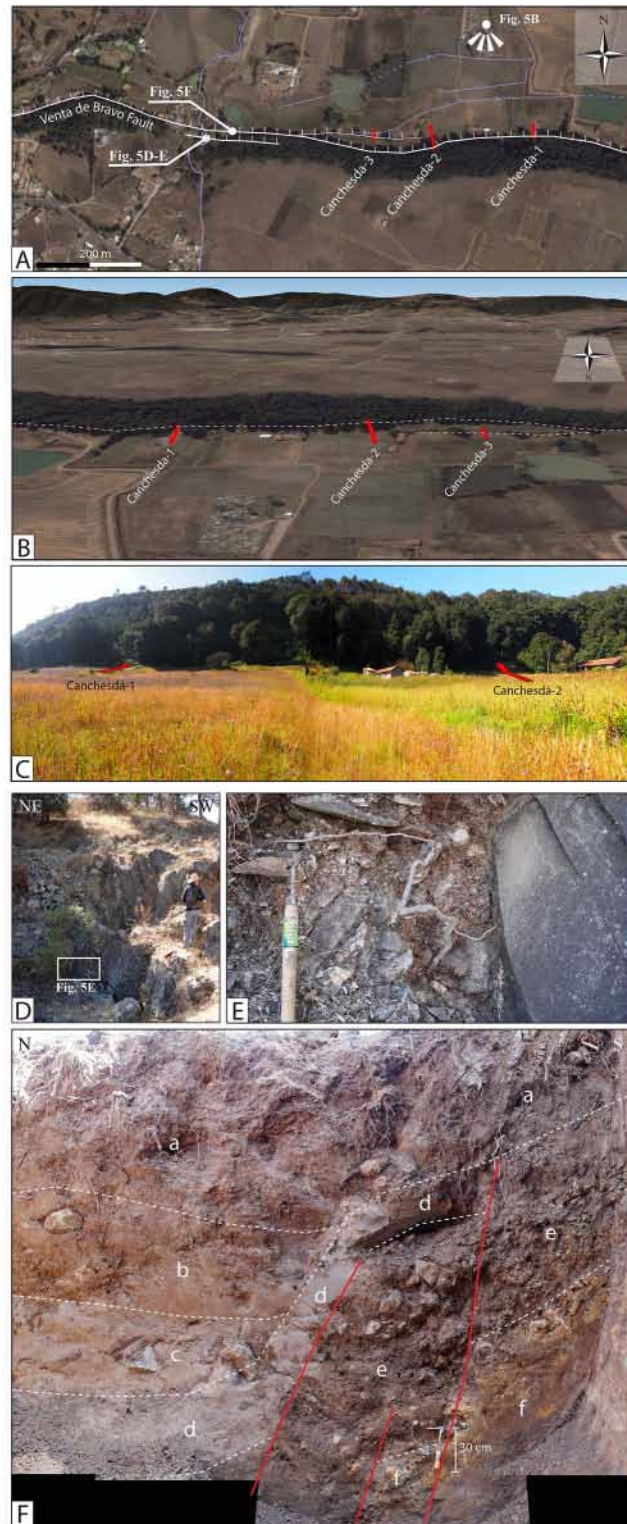
Figure 5. (a) A: Aerial photograph of the Canchesdá site along the Venta de Bravo Fault (VBF), red rectangles indicate the location of trenches. B: Oblique aerial view showing the trace and the two splays of the VBF at the Canchesdá site (derived from Google Earth). C: Picture of the scarp showing the location of Canchesdá-1 and Canchesdá-2 trenches. (b) D: Fault plane within a second order tributary of the Lerma River. E: Detail of striated fault plane. F: Exploratory trench Canchesdá-4 excavated to the east of Can-creek exposure.

Table 3
Sedimentary Description and Genetic Interpretation of the Units Exposed in the Trench Walls of Canchesdá Trench Site

Units	Description	Interpretation
U1	20–50 cm of remobilized pumice and brown organic matter with some blocks of andesite	Present day soil
U2	80–120 cm thick matrix-supported layer of andesite blocks derived from the main fault scarp, occasional pumice in light-brown clay rich and sandy matrix. Paleosoil on top with pieces of ceramics within	Slope deposit
U3	60–80 cm of dark-brown to pale-yellow lapilli size pumice deposit, remobilized, weathered and highly oxidized with some andesitic blocks in organic matter. Discordant with U4	Epiclastic volcanic material (U4–U5)
U4	40–80 cm of pale-yellow to brown lapilli size pumice deposit, grain-supported, with normal grading. No evident primary lamination but contains secondary horizons rich in iron oxides. Concordant with U5	Fall deposits, Brown pumice
U5	Up to 2 m of pale-brown to yellow discontinuously laminated pumice deposits, <0.8 mm in size. Laminated tephra at the base. Presence of sparse small andesitic lithics and red scoria. Concordant contact with the unit below (U6)	Fall deposits, yellow pumice
U6	Conglomerate made of matrix supported up to 40 cm andesitic blocks in a brownish sandy-pebble rich matrix. The base is not exposed in the trench wall	Colluvial deposit

dip-slip with a minor left-lateral component (Figures 5B-5E). This free face is partially covered with a thick colluvium that was sampled (sample VB02), even though it is not suitable for paleoseismological analysis. The colluvium is made of heterometric angular clasts (up to 30 cm) derived from the dacitic lavas that made the scarp.

3.2.2. Canchesdá Trench Stratigraphy

Unfortunately, As mentioned, we could not proceed with a paleoseismological analysis at Canchesdá-4 trench, since we only had access for a couple of hours. Photographs of the trench walls allowed us to identify six different units, which we can be partially described and interpreted as follows, from base to top, Unit F is an ignimbrite deposit with yellowish weathering. Unit E is composed by an heterometric colluvium with angular and sub-angular clasts derived from the lava deposits and up to 35–40 m in diameter. Unit D is a clayish deposit perhaps coming from the weathering of volcanic ashes. Units C, B and A are suspected edaphic horizons that form a 1.30 m thick colluvial deposit (Figure 5b-F). The paleoseismological study of the other 3 trenches (Canchesdá 1, 2 and 3) allowed to describe the general lithostratigraphy composed of volcanic, colluvial, and alluvial deposits with paleosols developed in between (Figure 6). The general stratigraphic column consists of six main units (U6–U1) described in Table 4.

The basal unit (U6) is exposed only in Canchesdá-2, and it is interpreted as a colluvial deposit covered by a thin, discontinuous layer of intensely deformed white-gray sand (Figure 6). The base of U6 is not exposed in the trench. A sample from this unit, Can 2-2, yielded an age of 25,980 ± 110 years BP. U6 is overlain in concordant contact by two pumice fall-out deposits forming yellow (U5) and brown (U4) units exposed in Canchesdá-1 and Canchesdá-3, while in Canchesdá-2 a sandy unit affected by liquefaction features lies between U6 and U3. The thickness of U5 varies drastically from 2 to 3 m in Canchesdá-1 to about 70 cm in Canchesdá-3, while it was not preserved or deposited in Canchesdá-2. The sample Can 3-1 yielded an age of 10,310 ± 30 years BP for the deposition age of U5 pumice. U4 is concordant and genetically related with U5 and should correspond to the same volcanic episode. The main difference among these units relies in the grade of weathering (distinctive colors) and the presence of different primary structures. The overlying discordant U3 corresponds to reworked material from the previous units, with an average thickness of 45 cm. Whereas in trenches 1 and 2 the unit maintains a relatively constant thickness, in trench 3 it shows abrupt changes in thickness, probably resulting from incision of small gullies draining a nearby creek located to the east (Figure 5A). Samples Can 1-2 and Can 3-7 from this unit yielded ages of 5,070 ± 30 years BP and 9,770 ± 30 years BP, respectively. U3 is overlaid by unit U2, which is a slope deposit containing lava blocks derived from the main scarp. U2 is present in the three trenches with a variable thickness because it is mostly covering an irregular topography likely resulting from an erosive episode as suggested by the presence of paleochannels on trenches 2 and 3. The samples Can 3-6 and Can 3-10 taken in U2 are ceramic shards and the sample Can 3-9 gave a radiometric age of 725 ± 30 years BP. At the top, overlaying the previous units, U1 corresponds to the present-day soil with an average thickness of ca. 15 cm.

3.3. Faulting and Deformations

The deformation observed in the trenches includes primary features such as faults offsetting units and secondary features such as open fissures, folding and liquefaction structures in sandy units. To describe the faults, we
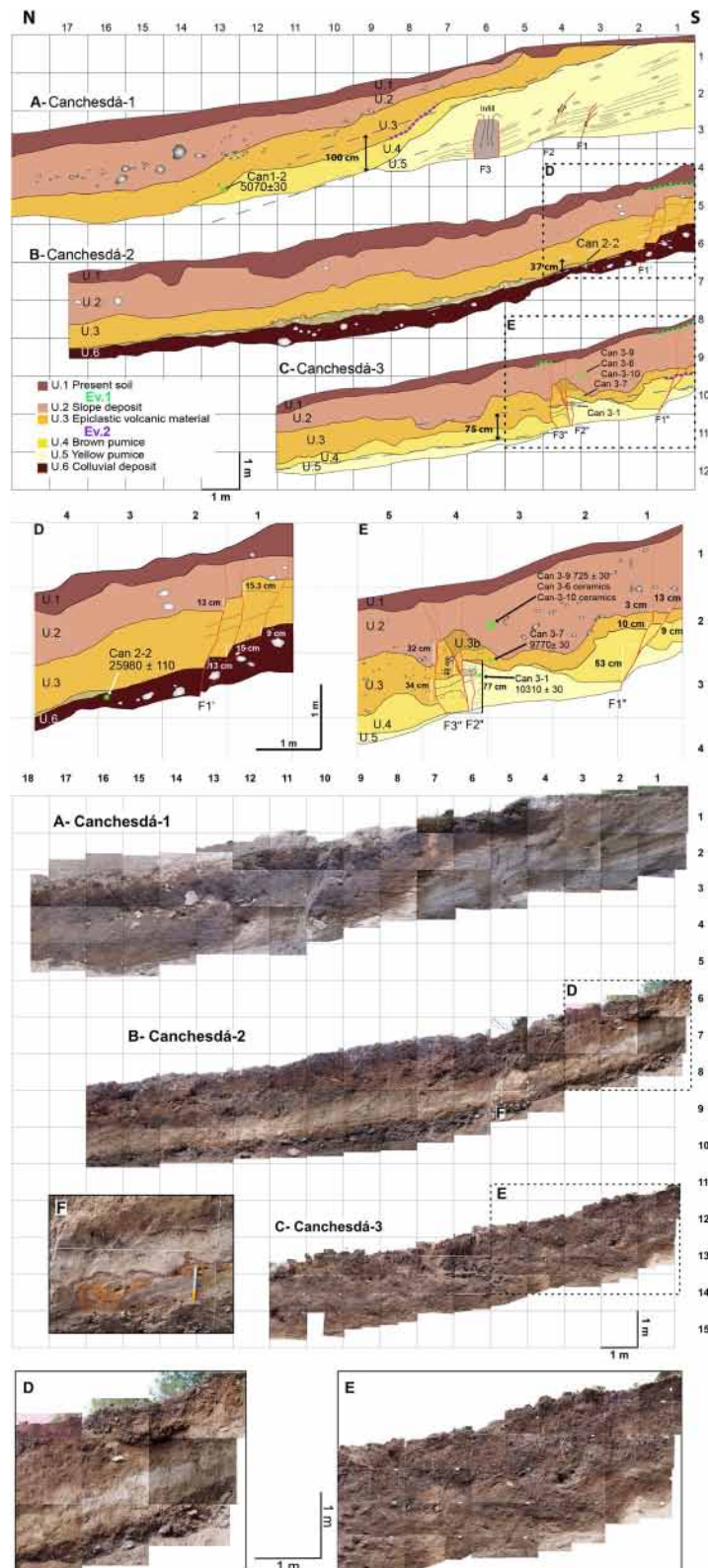
Figure 6. (a) Trench logs of the Canchesdá site. A: Canchesdá-1, B: Canchesdá-2, C: Canchesdá-3, D: Zoom of the faulted zone in Canchesdá-2, E: Zoom of the faulted zone in Canchesdá-3. Samples: green dot; event horizons: color dashed lines. (b) Photomosaic of the three trenches presented in (a) and a zoom in Canchesdá-2 showing liquefaction features.

Table 4
Dating Results

Sample name (Unit)	Type of material	Conventional age (year BP)	2σ calibrated age (cal year BP)
Can 1-2 (U3)	Charcoal	5,070 ± 30	5,910–5,735 (5,822 ± 87)
Can 2-2 (U6)	Bulk	25,980 ± 110	30,590–29,875 (30,232 ± 357)
Can 3-1 (U5)	Charcoal	10,310 ± 30	12,365–12,015 (12,190 ± 175)
Can 3-7 (U3)	Bulk	9,770 ± 30	11,235–11,180 (11,207 ± 27)
Can 3-9 (U2)	Bulk	725 ± 30	725–570 (647 ± 77)
Can Creek	Charcoal	2,430 ± 55	2,707–2,357 (2,532 ± 175)

Note. Ages calibrated using OxCal 4.2 software with 2σ uncertainty (Bronk Ramsey, 2009). All the results are rounded to the nearest multiple of 5.

named them from south to north as F1, F2, and F3 in Canchesdá-1, F1′ in Canchesdá-2 and F1″, F2″ and F3″ in Canchesdá-3. No striations have been found in the trench materials. The correlation of faults among trenches is not straightforward. Due to the limited outcrops and the distance between trenches, we can only suggest that F1′ in Canchesdá 2 probably corresponds to a different branch than F1″, F2″ and F3″ from Canchesdá 3 that is excavated across on a smaller scarp, north of the main 50–60 m fault scarp (Figure 5B).

Canchesdá-4 exposed three clear fault branches (oriented N80E) that affect the ignimbrite basal unit, the lower colluvial unit and the clayish deposit, showing a minimum displacement of up to 1 m, but adding all it may reach 2 m.

Canchesdá-1 exposed three faults F1, F2, and F3 that only affect U5 and do not reach the top of the unit. Along with F1 and F2, laminations of the pumice are displaced from 0.5 to 2 cm (Figure 6). F3 corresponds to a 70 cm wide open fracture without any evident vertical offset and filled with a mix of weathered pumice belonging to the same U5. The dip of units U5 and U4 sharply increases toward the north at columns 7 and 8 of the log (Figure 6a-A), showing a folding or a tilting which indicates that a major fault may lie underneath this zone. The angular discordance between these units and U3 indicates that this deformation occurred between the deposition of U4 and the formation of U3. Even if the trench did not expose a major fault, there is a partial exposure of a fold scarp.

In Canchesdá-2, only F1′ displaced units U6–U2 but it does not affect U1. From the trench bottom to the surface, F1′ splays into three branches vertically displacing U6 to U2 by 37 ± 0.5 cm (Figure 6a-B). In this trench, the top of U6 exhibits liquefaction features (Figure 6b). Considering the surface envelope of the contact U3–U6 the vertical displacement of 37 cm across the whole fault zone is confirmed (Figure 6a-C).

In Canchesdá-3, the faulting is more complex than in the other two trenches. Three subvertical E-W striking, north-dipping faults affect all units except the uppermost one (U1). The deeper units U5 and U4 are displaced along F1″ by 53 ± 0.5 cm, while U3 and U2 are only displaced by 16 ± 0.5 to 19 ± 0.5 cm. This pattern is repeated along F2″, where U5 and U4 are displaced by 77 ± 0.5 cm, while U3 and U2 are only displaced by 23 ± 0.5 cm. Locally, the relative homogeneity of U3 is disturbed at the level of F2″ by a mix of clayish materials which could correspond to a localized filling or alteration of U3 (U3b in Figure 6a-C). Along F3″, U3 and U2 are displaced by 34 ± 0.5 and 32 ± 0.5 cm. Considering the surface envelopes of the contact between U4 and U5, a vertical displacement of 75 cm across the whole fault zone is measurable at the scale of the trench (Figure 6a-C).

4. Discussion

4.1. Paleoseismic Interpretation

4.1.1. Age of Units

The units unveiled in the trenches ranged in age between ca. 30 kyr and 500 years and the ages of the samples are consistent with the stratigraphic order (Table 4). However, the ages of some units cover a wide time span, which could be interpreted as a record of intermittent sedimentation. The colluvial unit naturally exposed on the creek (Can-Creek, sample VB02) yielded an age of 2,532 ± 175 cal year BP. The U6 yielded an age of

30,232 ± 357 cal year BP. This unit might have been younger since this result comes from a bulk sample, which can contain recycled organic material in a colluvial environment (Table 3). The unit above, the U5 volcanic fall deposits, is dated with charcoal samples: U5 (Can 3-1; 12,190 ± 175 cal year BP). This age and description of this unit is consistent with the Plinian eruption of the Jocotitlan volcano located 25 km to the east of the trench site (Figure 2; Siebe et al., 1992). Covering U4 and U5, the unit U3 is dated with a charcoal sample at 5,822 ± 87 cal year BP (Can 1-2). We consider sample Can 3-7 (U3; 11,207 ± 27 cal year BP) as probably less representative of the age of U3 since it is a bulk sample that might contain resedimented charcoal, but it is still in the stratigraphic order.

At the top of the trench, the age obtained for U2 (647 ± 77 cal year BP) is consistent with the presence of ceramic artifacts in this early historical slope deposit. Although the age control of the sequence is limited, it seems to be the record of condensed sedimentation; the resistant scarp made of lavas has been eroded slowly and little material was supplied to the slope along the scarp interlayered with volcanic fall deposits.

4.1.2. Paleoseismic Events

By correlating the paleosurface ruptures, tilting, folding and cracks identified in the three trenches, two slip events can be interpreted, whose age constraint is provided in the retrodeformation section. Event 1 has a minimum slip per event (SPE) of 37 ± 1 cm (measured in Canchesdá-2) and the Event 2 has a minimum SPE of ca-1 m (measured in Canchesdá-1).

Event 1, is visible in the trenches Canchesdá-2 and Canchesdá-3, where all units except for U1 are affected (Figure 6). The SPE is about 37 ± 1 cm at the U3–U6 interface in Canchesdá-2. This displacement is unambiguous and measurable by adding the slip calculated across the different fault branches or by considering the displacement of the enveloped surface of the U3–U6 interface. The U2–U3 interface corresponding to an erosional contact is particularly irregular and does not allow tracing a correct envelope surface. The SPE should be considered a minimum value, which is likely to be increased by the addition of other small displacements not exposed in the trench but located in other branches, especially the main fault branch to the south of it. Indeed, we cannot exclude that the fault zone is wider and extends to the south since the faults exposed in Canchesdá-2 are next to the southern end of the trench, at the foot of the ca. 50 m high topographic scarp. In Canchesdá-3, distinguishing the SPE of Event 1 and Event 2 is not straightforward due to the irregular contacts between units, the complexity of the fault branches, and due to the presence of what we interpret as a tilted block (Figure 6E). The 75 cm offset of the envelope surface was measured at the U4–U5 interface, thus accumulating the effect of the two events (Figure 6C). If we add the slip observed on each individual fault branch, we obtain a summed offset of 130 cm. This difference in offset compared with the one derived from the envelope can be explained by the fact that the 130 cm is reflecting the tilting of the block located between the two fault zones F1″ and F2″–F3″ (at columns 2–4), which is a local effect. The U3–U4 and U2–U3 interfaces are particularly irregular (non-planar erosion surfaces) not allowing us to calculate the offset associated with each event at the scale of the trench, and only the cumulative displacement of ca. 75 cm by the two events is measurable.

Event 1, which occurred between the formation of U2 and U1, is interpreted as a paleoseismic event since the vertical displacement is unambiguous in the two trenches. The older one, Event 2, occurred between the deposition of U4 and U3. It is defined in Canchesdá-3 by a greater displacement of U4 and of older units along F1″ and F2″ (53 cm along F1″) than of U3–U2 (between 13 and 22 cm along F1″). By subtracting the displacement related to Event 1, the associated displacement is about 34 ± 0.5 cm along F1″ and 14 ± 0.5 cm along F2″–F3″ (see retrodeformation discussion for detail). This latter offset cannot be taken as representative of the in-depth SPE, but as an apparent exaggeration by the tilting of the central block.

One of these two events could be responsible for the liquefaction features visible at the top of U6 in Canchesdá-2 and corresponding to a moderate to large ground shaking postdating the unit formation (Figure 6a-B).

In Canchesdá-1, the fissure and small faulting of U5 along F1, F2, and F3 are likely to be the consequences of the folding or tilting of U5 and U4. This geometry is typical of drape folds. Such draped folds are quite common in faults affecting volcanic material with low compaction degrees (e.g., Berryman et al., 2022; Jomard et al., 2021; Lacan et al., 2018).

Since the U3–U4 interface was partially eroded we use the envelope surface of the U4–U5 interface to estimate the vertical deformation considering the bottom of the trench as the highest possible location of it in the hanging
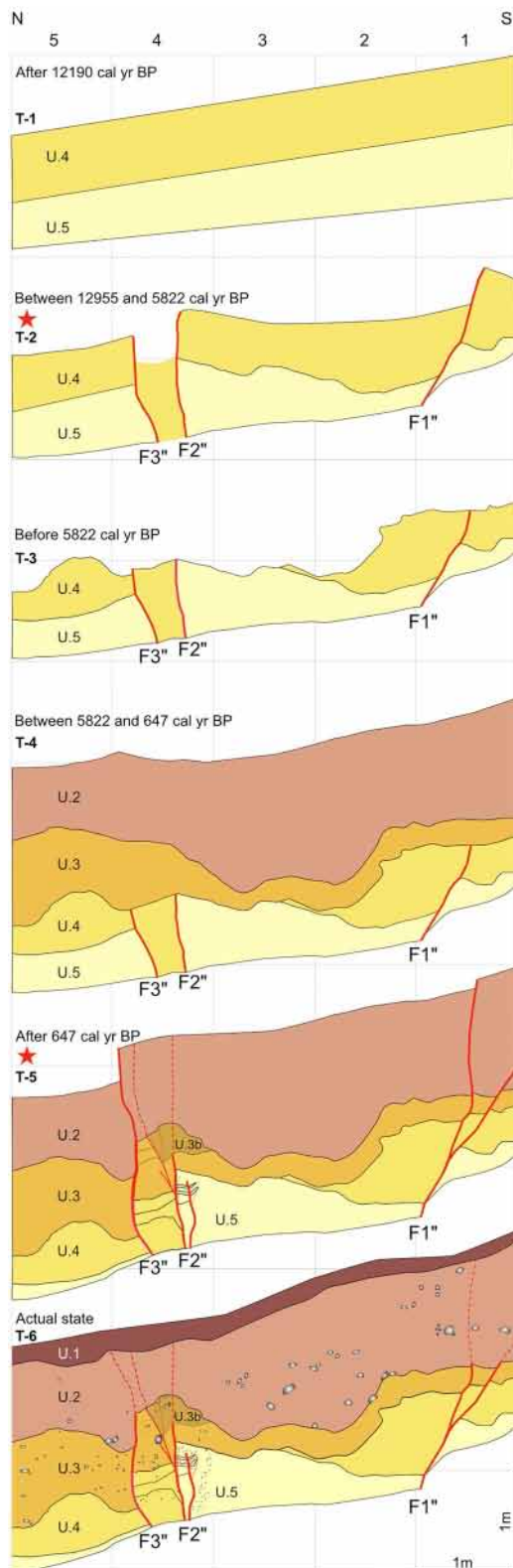
Figure 7. Retrodeformation steps of the Canchesdá-3 trench illustrating the most likely interpretation. The red stars at T-2 and T-5 represent the periods during which seismic events occurred. Red lines are the faults.

wall. The envelope is affected by a minimum offset of ca. 100 cm during Event 2. The future excavation of larger trenches in this area could shed light in this interpretation and measure the total displacement related to this event. In any case, we consider this as additional evidence for Event 2, occurred between U4 and U3 deposition.

4.1.3. Retrodeformation Analysis

The Canchesdá-3 trench was retro-deformed to illustrate and analyze the timing and extent of deformation during each event in the most probable scenario (Figure 7). Two ruptures have been identified in that trench affecting U5–U4 and U5–U2, respectively. Considering the main episodes of erosion, sedimentation, or tectonics, six time-lapses are defined, occurring between $12{,}190 \pm 175$ cal year BP and the present as follows:

T-1: During $12{,}190 \pm 175$ cal year BP, a pumice fall-out deposit (units U5 and U4), mantled a topographic surface gently dipping north.

T-2: Event 2 occurred between $12{,}190 \pm 175$ and $5{,}822 \pm 87$ cal year BP and is associated with an accumulated surface displacement of ca 34 cm along F1″ while the movement recorded on F2″–F3″ seems to correspond to a fracture opening.

T-3: After Event 2 and before the sedimentation of U3 (reworked volcanoclastic material dated at $5{,}822 \pm 87$ cal year BP), parts of U4 and U5 were partially eroded, and the fault scarp was smoothed.

T-4: The resulting eroded topography was filled with U3 and U2 during a time lapse between $5{,}822 \pm 87$ and 647 ± 77 cal year BP. U3 underwent local erosion, probably related to the incision of small gullies, especially around Canchesdá-3 area. Then, this unit was covered gradually with slope deposits forming U2.

T-5: The last seismic event (Event 1) occurred between units 2 and 1, that is, between 647 ± 77 cal year BP and 250 years BP. This last age corresponds to the beginning of the period for which the historical seismicity record is complete for $M > 6$ earthquakes in this region (García Acosta & Suárez, 1996; Suárez et al., 2019). After this date, only one document mentions a series of small earthquakes that were felt in Tlalpujahua, located 6 km south of the VBF, between March 1745 and November 1746 (Sahagún de Arévalo Ladrón de Guevara, 1746). However, there is no description of the loss of life or damage, making it improbable to be related to the surface rupture of Event 1. Accordingly, we consider that this event occurred after 647 ± 77 cal year BP (1303 ± 77 AD) and before 1700 AD, the beginning of the period of completeness of the historical seismicity catalog for $M > 6$ earthquakes.

T-6: During the last stage, the current soil (U1) was formed.

4.2. Paleoseismic Parameters

The three trenches at the Canchesdá site exposed the paleoseismic history of the eastern segment of the VBF for the last 12 ka. The two identified events yield a rough recurrence interval between 5.5 and 11.5 ka. This value is 2–5 times lower than that one estimated at the western tip of the VBF, which is 2.1 ± 0.2 ka (Lacan et al., 2018). This difference could be explained by different aspects: (a) the poor quality of statistics performed with only two recorded events; (b) the fact that the trenches recorded the earthquake history on only one or two fault branches in a place where more fault branches are suspected. Accordingly, other paleoearthquakes could have ruptured in parallel fault branches without being recorded. The differences in recurrence
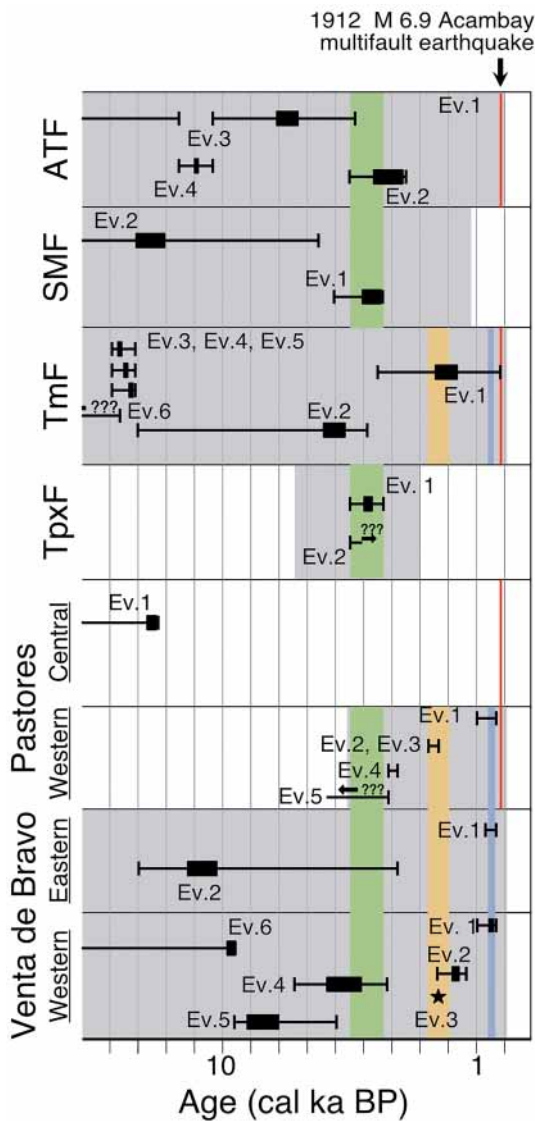
Figure 8. Paleoseismic events of the last 15 ka identified in the Acambay Graben. Gray zone: complete sedimentary record. White zone: incomplete sedimentary record. Color bars indicate a correlation of simultaneous ruptures. ATF, Acambay-Tixmadeje Fault; SMF, San Mateo Fault; TemF, Temascalcingo Fault; TepF, Tepuxtepec Fault; PF, Pastores Fault; VBF, Venta de Bravo Fault.

time might also suggest that the VBF fault does not always rupture along its entire length. The value is also lower than the recurrence time calculated for the western tip of the PF by Ortuño et al. (2015), which is estimated between 1.1 and 2.6 ka, where secondary and not only primary surface ruptures have been recorded.

The vertical SPE in the Canchesdá site ranges from 37 to 100 cm. The vertical displacement measured for Event 1 is about 37 ± 1 cm in Canchesdá-2. The vertical displacement for Event 2 measured in Canchesdá-1 is at least 100 cm by considering the offset of the U4–U5 interface. By considering the uncertainty of the age of Event 2 (between $12,190 \pm 175$ and $5,822 \pm 87$ cal year BP), the minimum dip slip-rate ranges from 0.1 to 0.23 mm/year for the last 12 ka. This slip rate must be considered as a minimum since the rupture only corresponds to a part of the whole fault zone. Moreover, other events, likely not recorded on the studied branches, may have happened along other fault branches.

Because of the uncertainty on the coseismic vertical displacement associated with those earthquakes, the paleomagnitudes have been estimated using the SRL by means of Wesnousky (2008) scaling relationship derived for normal faults in volcanic context (Stirling et al., 2002). Three potential magnitudes of $M_W 6.75 \pm 0.27$, $M_w = 6.91 \pm 0.27$ and $M_w = 7.01 \pm 0.27$ have been estimated by considering SRL of 22 km for the eastern VBF segment, 48 km for the entire VBF and 80 km for the full extension of PF and VBF taken together. The likelihood of such ruptures will be discussed below by correlating rupture events identified in the previous studies.

4.3. Multi-Fault Rupture Events Within the Acambay Graben

The compilation of paleoseismic events recorded at different sites of the Acambay graben allows to analyze the existence of common feasible ruptures by comparing different sites. This analysis does not mean that we are able to correlate in a robust way the surface ruptures, but just opens the possibility of rejecting or considering their feasibility. Depending on sedimentary record preservation and the availability of suitable samples for dating, the age estimated for paleoearthquakes in the Acambay graben varies from about 10 years to more than a thousand years (Figure 8). In such period, various earthquakes can occur producing surface ruptures that can be wrongly correlated among them. Considering the possible correlation of surface ruptures between trenches is challenging but nevertheless necessary for estimating the seismic hazard, since magnitude is related to the SRL. Indeed, the two known historical earthquakes associated with surface ruptures that have occurred in the TMVB correspond to multi-fault ruptures (the Ameca and the Acambay earthquakes; Lacan & Arango-Galván, 2021; Núñez-Meneses et al., 2021;

Suárez et al., 1994; Suter, 2015b; Suter et al., 1995; Urbina & Camacho, 1913). In such a context, ignoring such possibilities to interpret paleoseismic data and only considering individual fault ruptures would wrongly underestimate the regional seismic hazard.

The temporal distribution of the paleoseismological events for the last 15 ka is shown in Figure 8 and Table 2. These events were identified at eight fault segments belonging to three different fault systems within the graben (Acambay fault system, Temascalcingo-Tepuxtepec fault system, and the PVBFS). From the comparison chart, we can infer that four of the events (colored in red, blue, orange and green) could have occurred simultaneously in the three systems. Even if dealing with large age uncertainties that do not allow us to determine that these correlations reflect co-seismic ruptures, we think such possible large and multi-rupture scenarios should be considered when assessing probabilistic hazard assessment in the region until we can discard them with direct observations.
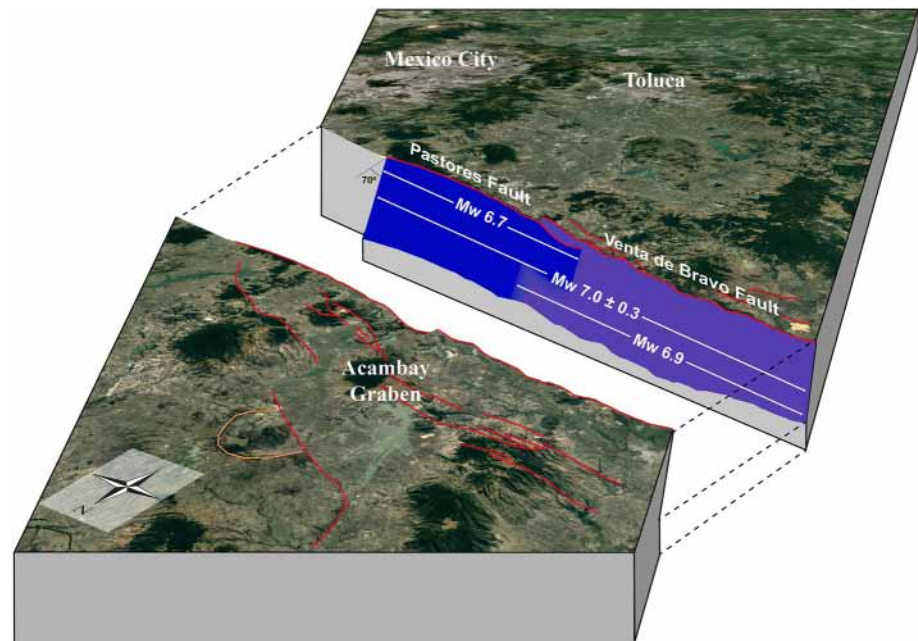
Figure 9. Block diagram of the Acambay Graben showing the connection between the Venta de Bravo fault (Purple) and the Pastores fault planes (Blue). The cartographic trace of the faults is represented in red, and the biggest cities are located on the 3D view extracted from Google Earth.

4.3.1. Paleorupture of the Pastores-Venta de Bravo Fault System

The compilation of paleoearthquakes in the Acambay Graben (Figure 8), shows that the Ev.1 recorded at Canchesdá (647–250 cal year BP; this paper) might have corresponded with the Ev.1 recorded along the western VBF (924–250 cal year BP; Lacan et al., 2018) and along the western PF (960–250 cal year BP; Ortuño et al., 2015). For the last tectonic deformation recorded along the western PF, Ortuño et al. (2015) tentatively attributed this recent event to the 1912 Acambay earthquake. However, according to Urbina and Camacho (1913), the rupture along the PF during the 1912 earthquake is limited to the east of "Puertecito," 10 km east of the Laguna Bañí trench site of Ortuño et al. (2015) (Figure 2). In our opinion, it is more likely that the Ev.1 recorded along the western PF correlates with a surface rupture recorded in VBF which occurred between 647 and 250 cal year BP. If this multi-fault rupture scenario is confirmed, it would mean that a rupture along the PF and VBF occurred in prehistoric to early historical times (Figure 8).

The possibility of a simultaneous rupture along the PF and VBF is supported by considering that the two faults overlap for about 13 km and are separated by a relay zone of only 1 km width. Such a distance, according to Biasi and Wesnousky (2016, 2017), should not represent a real impediment to fracture propagation. Also, Boncio, Lavecchia, Milana, et al. (2004), based on a complete study of the behavior of normal faults in Italy, recommend not considering two fault segments that are aligned and display a step over ≤4 km as different seismogenic segments.

A rupture along the entire southern border of the Acambay Graben implies a possibility of M_w 7.0 ± 0.3 earthquakes and allows highlighting one of the greatest potential seismic sources located at less than 70 km from the super populated Mexico City, as well as from other large cities such as Toluca, Morelia, Celaya, San Juan del Rio and Querétaro (Figures 1 and 9). The effect of such a large earthquake occurring close to urban centers is illustrated by the devastating effects in Mexico City caused by the recent 19 September 2017, $M_w = 7.1$ Puebla-Morelos earthquake (57 km depth), which generated 0.5 g acceleration in the lacustrine basement of Mexico City (Iglesias et al., 2018; Pérez-Campos et al., 2017; Sahakian et al., 2018). In the case of such an event occurring at the PVBFS, given that the hypocenter should be shallower, the expected ground motion acceleration at similar distances would be similar (Suárez & Jaimes, 2023) or even higher (Díaz-Mojica et al., 2018).

4.3.2. Other Possible Multi-Fault Ruptures

Further back in time than the last millennial, uncertainty on the event ages makes the rupture correlation more hazardous. However, ruptures observed along the western VBF, the western PF and the Temascalcingo fault

at around 2.2–2.7 ka BP (orange line in Figure 8) could also indicate a rupture of about 80 km. With even more uncertainty, another possible rupture correlation was identified by Sunye-Puchol et al. (2015) along the Acambay-Tixmadeje and San Mateo Fault in the period between 4.2 and 5.5 ka BP (green line in Figure 8).

Our results indicate that the multi-fault ruptures occurred in the 1912, along three fault system of the graben, could not be the only ones to have affected the region in prehistorical or early historical times. Such rupture modes imply a strong interaction of faults that belong to the same system and could explain the variable rupture behavior identified by Ortuño et al. (2019) along the Temascalcingo-Acámbaro Fault System. Finally, we remark that multi-fault rupture events of $M_w \sim 7$ could have terrible consequences for the densely populated TMVB region, in particular in the central sector. Although individual recurrences may reach several hundred or even thousands of years, the contribution of as many potential sources as possible and their integration into hazard calculations is essential for a better estimation of the risk to the population.

5. Conclusions

The paleoseismic evidence obtained during this work provides new constraints about the Holocene tectonic activity of the eastern segment of the VBF, a bounding fault system of the Acambay Graben in the TMVB. The Canchesdá trenches exposed volcanic and colluvial deposits affected by normal faulting along fault branches synthetic to the main VBF eastern segment. Two paleoseismic events are interpreted from discrete displacements, folding and filled open fractures. The older Event 2 occurred between $12{,}190 \pm 175$ and $5{,}822 \pm 87$ cal year BP and the younger Event 1 occurred between 647 ± 77 and 250 cal year BP. Paleoseismic parameters indicate a minimum slip-rate of 0.1 and 0.23 mm/year for the last 12 ka with a recurrence interval of 8.5 ± 3 ka. Even though these parameters are consistent with the ones calculated along with other faults in the region, they are likely underestimated since two events are insufficient to estimate a recurrence interval and the slip-rate calculated along some fault branches might not be necessarily representative of the total fault zone displacement.

Correlations between the two events recognized in Canchesdá trenches with other paleo-events identified previously on other faults of the graben, confirm that the multi-fault rupture event of 1912 is certainly not exceptional and that other similar or perhaps bigger earthquakes have probably already occurred in the past. One of these multi-rupture seismic events may have occurred between 647 and 250 cal year BP, breaking along both VBF and PF. A potential future earthquake involving the whole PF and VBF would produce a M_w 7.01 ± 0.27 earthquake (Figure 9).

The correlations of cluster events that could correspond to $M_w > 7$ multi-fault ruptures indicate a recurrence interval of 600 to 1,200 years at the scale of the graben.

We identified the PVBFS as the potentially largest seismogenic source within the 100 km radius of Mexico City (Figure 9). Considering the proximity between the active fault system and the megacity, the potential magnitude and a depth shallower than 20 km, the associated damage could be catastrophic for the population and the infrastructure, even surpassing that observed during the 19 September 2017 earthquake.

Data Availability Statement

The Hillshade imagery utilized in Figures 1 and 4a can be accessed freely from the Instituto Nacional de Estadística y Geografía (INEGI, 2022). The digital elevation model GMRT employed in Figures 2 and 4b originates from GeoMapApp (Ryan et al., 2009). The epicenters displayed in Figure 1 were acquired from the catalog of the Servicio Sismológico Nacional (http://www.ssn.unam.mx/). The slab contours depicted in Figure 1 were derived from the Slab v.2 dataset (Hayes, 2018). The polygons representing urban areas in Figure 1 were obtained from CONABIO (2015).

References

Abe, K. (1981). Magnitudes of large shallow earthquakes from 1904 to 1980. *Physics of the Earth and Planetary Interiors*, *27*(1), 72–92. https://doi.org/10.1016/0031-9201(81)90088-1

Aguirre-Díaz, G. J., Urrutia-Fucugauchi, J., Soler-Arechalde, A. M., & McDowell, F. W. (2000). Stratigraphy, K-Ar ages, and magnetostratigraphy of the Acambay graben, central Mexican Volcanic Belt. In *Special Papers-Geological Society of America* (Vol. 334, pp. 167–178). https://doi.org/10.1130/0-8137-2334-5.167

Arzate, J., Lacan, P., Corbo-Camargo, F., Arango-Galván, C., Felix-Maldonado, R., Pacheco, J., & León-Loya, R. (2018). Crustal structure of the eastern Acambay Graben, central Mexico, from integrated geophysical data. *Revista Mexicana de Ciencias Geológicas*, *35*(3), 228–239. https://doi.org/10.22201/cgeo.20072902e.2018.3.864

Audemard, M. F. A. (2005). Paleoseismology in Venezuela: Objectives, methods, applications, limitations and perspectives. *Tectonophysics*, *408*(1–4), 29–61. https://doi.org/10.1016/j.tecto.2005.05.034

Berryman, K., Villamor, P., Nairn, I., Begg, J., Alloway, B. V., Rowland, J., et al. (2022). Volcano-tectonic interactions at the southern margin of the Okataina Volcanic Centre, Taupō Volcanic Zone, New Zealand. *Journal of Volcanology and Geothermal Research*, *427*(November 2021), 107552. https://doi.org/10.1016/j.jvolgeores.2022.107552

Biasi, G. P., & Wesnousky, S. G. (2016). Steps and gaps in ground ruptures: Empirical bounds on rupture propagation. *Bulletin of the Seismological Society of America*, *106*(3), 1110–1124. https://doi.org/10.1785/0120150175

Biasi, G. P., & Wesnousky, S. G. (2017). Bends and ends of surface ruptures. *Bulletin of the Seismological Society of America*, *107*(6), 2543–2560. https://doi.org/10.1785/0120160292

Boncio, P., Lavecchia, G., Milana, G., & Rozzi, B. (2004). Seismogenesis in Central Apennines, Italy: An integrated analysis of minor earthquake sequences and structural data in the Amatrice-Campotosto area. *Annals of Geophysics*, *47*(6), 1723–1742. https://doi.org/10.4401/ag-7227

Boncio, P., Lavecchia, G., & Pace, B. (2004). Defining a model of 3D seismogenic sources for Seismic Hazard Assessment applications: The case of central Apennines (Italy). *Journal of Seismology*, *8*(3), 407–425. https://doi.org/10.1023/B

Bronk Ramsey, C. (2009). Bayesian analysis of radiocarbon dates. *Radiocarbon*, *51*(1), 337–360. https://doi.org/10.1017/S0033822200033865

CONABIO. (2015). Manchas urbanas y rurales [Dataset]. Retrieved from http://www.conabio.gob.mx/informacion/gis/

De Mountessus De Ballore, C. (1913). The Mexican earthquake of November 12, 1992. *Boletín Del Instituto de Geología de México*, *32*, 31–33.

Díaz-Mojica, J. J., Cruz-Atienza, V. M., Villafuente Urbina, C. D., Tago Pacheco, J., & Lacan, P. (2018). Generación de registros sintéticos en la estación de C.U. para sismos corticales en la parte central de México. In *Reunion Anual Union Geofísica Mexicana. Puerto Vallarta, Jalisco, México*. Retrieved from https://raugm.org.mx/2018/resumenes/sessions/abstract.php?abstractID=794&source=session

Ferrari, L., Orozco-Esquivel, T., Manea, V., & Manea, M. (2012). The dynamic history of the Trans-Mexican Volcanic Belt and the Mexico subduction zone. *Tectonophysics*, *522–523*, 122–149. https://doi.org/10.1016/j.tecto.2011.09.018

Ferrari, L., Pasquarè, G., & Tibaldi, A. (1990). Plio-Quaternary tectonics of the central Mexican Volcanic Belt and some constraints on its rifting mode. *Geofísica Internacional*, *29*(1), 5–18. https://doi.org/10.22201/igeof.00167169p.1990.29.1.614

Ferrari, L., Pasquare, G., Venegas-Salgado, S. S., Romero-Ríos, F., Pasquarè, G., Venegas-Salgado, S. S., & Romero-Ríos, F. (1999). Geology of the western Mexican Volcanic Belt and adjacent Sierra Madre Occidental and Jalisco block. In *Geology Society of America, Special Papers (Cenozoic tectonics and volcanism of Mexico)* (pp. 65–83). https://doi.org/10.1130/0-8137-2334-5.65

Fletcher, J. M., Teran, O. J., Rockwell, T. K., Oskin, M. E., Hudnut, K. W., Mueller, K. J., et al. (2014). Assembly of a large earthquake from a complex fault system: Surface rupture kinematics of the 4 April 2010 El Mayor-Cucapah (Mexico) Mw 7.2 earthquake. *Geosphere*, *10*(4), 797–827. https://doi.org/10.1130/GES00933.1

Fletcher, J. M., Teran, O. J., Rockwell, T. K., Oskin, M. E., Hudnut, K. W., Spelz, R. M., et al. (2020). An analysis of the factors that control fault zone architecture and the importance of fault orientation relative to regional stress. *GSA Bulletin*, *132*(9–10), 2084–2104. https://doi.org/10.1130/B35308.1

García Acosta, V., & Suárez, G. (1996). *Los sismos en la historia de México*. Universidad Nacional Autónoma de México. Retrieved from https://elfondoenlinea.com/Detalle.aspx?ctit=061012EA

Gómez-Tuena, A., Orozco-Esquivel, M. T., & Ferrari, L. (2007). Igneous petrogenesis of the Trans-Mexican Volcanic Belt. In *Special paper 422: Geology of México: Celebrating the centenary of the Geological Society of México* (Vol. 442, pp. 129–181). Geological Society of America. https://doi.org/10.1130/2007.2422(05)

Hayes, G. P. (2018). Slab2 - A comprehensive subduction zone geometry model [Dataset]. ScienceBase-Catalog. https://doi.org/10.5066/F7PV06JNV

Iezzi, F., Mildon, Z., Walker, J. F., Roberts, G., Goodall, H., Wilkinson, M., & Robertson, J. (2018). Coseismic throw variation across along-strike bends on active normal faults: Implications for displacement versus length scaling of earthquake ruptures. *Journal of Geophysical Research: Solid Earth*, *123*(11), 9817–9841. https://doi.org/10.1029/2018JB016732

Iglesias, A., Ordaz, M., Arroyo, D., Singh, S. K., Cruz-Atienza, V., Reinoso, E., et al. (2018). Deadly intraslab Mexico earthquake of 19 September 2017 (M_w 7.1): Ground motion and damage pattern in Mexico City. *Seismological Research Letters*, *89*(6), 2193–2203. https://doi.org/10.1785/0220180159

INEGI. (2022). Continuo de Elevaciones Mexicano [Dataset]. Retrieved from http://www.inegi.org.mx/app/geo2/elevacionesmex

Johnson, C. A., & Harrison, C. G. A. (1990). Neotectonics in central Mexico. *Physics of the Earth and Planetary Interiors*, *64*(2–4), 187–210. https://doi.org/10.1016/0031-9201(90)90037-x

Jomard, H., Saqui, D., Baize, S., Alvarado, A., Bernard, B., Audin, L., et al. (2021). Interactions between active tectonics and gravitational deformation along the Billecocha fault system (Northern Ecuador): Insights from morphological and paleoseismological investigations. *Journal of South American Earth Sciences*, *111*(May), 103406. https://doi.org/10.1016/j.jsames.2021.103406

Lacan, P., & Arango-Galván, C. (2021). Geophysical evidence of the 1912 earthquake rupture along the central fault system of the Acambay Graben, Central Mexico. *Boletín de La Sociedad Geológica Mexicana*, *73*(2), A250121. https://doi.org/10.18268/BSGM2021v73n2a250121

Lacan, P., Ortuño, M., Audin, L., Perea, H., Baize, S., Aguirre-Díaz, G., & Zúñiga, F. R. (2018). Sedimentary evidence of historical and prehistorical earthquakes along the Venta de Bravo fault system, Acambay Graben (Central Mexico). *Sedimentary Geology*, *365*, 62–77. https://doi.org/10.1016/j.sedgeo.2017.12.008

Langridge, R. M., Persaud, M., Zúñiga, F. R., Aguirre-Díaz, G. J., Villamor, P., & Lacan, P. (2013). Preliminary paleoseismic results from the Pastores fault and its role in the seismic hazard of the Acambay graben, Trans-Mexican Volcanic Belt, México. *Revista Mexicana de Ciencias Geológicas*, *30*(3), 463–481.

Langridge, R. M., Weldon, R. J., II, Moya, J. C., & Suárez, G. (2000). Paleoseismology of the 1912 Acambay earthquake and the Acambay-Tixmadejé fault, Trans-Mexican Volcanic Belt. *Journal of Geophysical Research*, *105*(B2), 3019–3037. https://doi.org/10.1029/199JB900239

León-Loya, R., Perea, H., Lacan, P., Ortuño, M., & Zúñiga, R. (2022). Evaluating the Coulomb static stress change and fault interaction in an extensional intra-volcanic arc: 1000 years of earthquake history in the Acambay Graben, Trans-Mexican Volcanic Belt. *Journal of South American Earth Sciences*, *117*(June), 103901. https://doi.org/10.1016/j.jsames.2022.103901

Martínez-Reyes, J., & Nieto-Samaniego, Á. F. (1990). Efectos geológicos de la tectónica reciente en la parte Central de México. *Universidad Nacional Autónoma de México, Instituto de Geología, Revista*, *9*(1), 33–50.

McCalpin, J. P. (2009). *Paleoseismology in extensional tectonic environments*. In *International geophysics* (2nd ed., Vol. 95). Elsevier Inc. https://doi.org/10.1016/S0074-6142(09)95003-3

Mildon, Z. K., Toda, S., Faure Walker, J. P., & Roberts, G. P. (2016). Evaluating models of Coulomb stress transfer: Is variable fault geometry important? *Geophysical Research Letters*, *43*(24), 12407–12414. https://doi.org/10.1002/2016GL071128

Núñez-Meneses, A., Lacan, P., Zúñiga, F. R., Audin, L., Ortuño, M., Rosas Elguera, J., et al. (2021). First paleoseismological results in the epicentral area of the sixteenth century Ameca earthquake, Jalisco – México. *Journal of South American Earth Sciences*, *107*(September 2020), 103121. https://doi.org/10.1016/j.jsames.2020.103121

Ortuño, M., Corominas, O., Villamor, P., Zúñiga, R. F., Lacan, P., Aguirre-Díaz, G., et al. (2019). Evidence of recent ruptures in the central faults of the Acambay Graben (central Mexico). *Geomorphology*, *326*(July), 17–37. https://doi.org/10.1016/j.geomorph.2018.07.010

Ortuño, M., Zúñiga, F. R., Aguirre-Díaz, G. J., Carreón-Freyre, D., Cerca, M., & Roverato, M. (2015). Holocene paleo-earthquakes recorded at the transfer zone of two major faults: The Pastores and Venta de Bravo faults (Trans-Mexican Volcanic Belt). *Geosphere*, *11*(1), 160–184. https://doi.org/10.1130/GES01071.1

Pasquaré, G., Garduño, V. H., Tibaldi, A., & Ferrari, M. (1988). Stress pattern evolution in the central sector of the Mexican Volcanic Belt. *Tectonophysics*, *146*(1–4), 353–364. https://doi.org/10.1016/0040-1951(88)90099-6

Pérez-Campos, X., Singh, S. K., Arroyo, D., Cruz-Atienza, V. M., Ordaz, M., Hjorleifsdottir, V., & Iglesias, A. (2017). The deadly Morelos-Puebla, Mexico intraslab earthquake of 19 September 2017 (Mw7.1): Was the earthquake unexpected and were the ground motions and damage pattern in Mexico City abnormal? In *American Geophysical Union, fall meeting 2017, abstract #S33G-2950*. Retrieved from http://adsabs.harvard.edu/abs/2017AGUFM.S33G2950P

Rodríguez-Pascua, M. A., Pérez-López, R., Garduño-Monroy, V. H., Perucha, M. A., & Israde-Alcántara, I. (2017). Estimation of the epicentral area of the 1912 Acambay earthquake (M 6.9, Mexico) determined from the earthquake archaeological effects (EAE) and the ESI07 macroseismic scale. *Quaternary International*, *451*, 74–86. https://doi.org/10.1016/j.quaint.2017.06.045

Ryan, W. B. F., Carbotte, S. M., Coplan, J. O., O'Hara, S., Melkonian, A., Arko, R., et al. (2009). Global multi-resolution topography synthesis [Dataset]. Geochemistry, Geophysics, Geosystems, *10*(3), n/a. https://doi.org/10.1029/2008GC002332

Sahagún de Arévalo Ladrón de Guevara, J. F. (1746). Gazeta de Mexico. Retrieved from https://hndm.iib.unam.mx/consulta/publicacion/visualizar/558075be7d1e63c9fea1a2af?intPagina=1&tipo=publicacion&anio=1735&mes=6&dia=1

Sahakian, V. J., Melgar, D., Quintanar, L., Ramírez-Guzmán, L., Pérez-Campos, X., & Baltay, A. (2018). Ground motions from the 7 and 19 September 2017 Tehuantepec and Puebla-Morelos, Mexico, earthquakes. *Bulletin of the Seismological Society of America*, *108*(6), 3300–3312. https://doi.org/10.1785/0120180108

Siebe, C., Komorowski, J., & Sheridan, M. F. (1992). Morphology and emplacement of an unusual debris-avalanche deposit at Jocotitlán volcano, Central Mexico. *Bulletin of Volcanology*, *54*(7), 573–589. https://doi.org/10.1007/BF00569941

SSN. (2022). Catálogo de sismos | UNAM, México. (n.d.) [Dataset]. Retrieved from http://www2.ssn.unam.mx:8080/catalogo/#. https://doi.org/10.21766/SSNMX/EC/MX

Stirling, M., Rhoades, D., & Berryman, K. (2002). Comparison of earthquake scaling relations derived from data of the instrumental and preinstrumental era. *Bulletin of the Seismological Society of America*, *92*(2), 812–830. https://doi.org/10.1785/0120000221

Suárez, G., Caballero-Jiménez, G. V., & Novelo-Casanova, D. A. (2019). Active crustal deformation in the Trans-Mexican Volcanic Belt as evidenced by historical earthquakes during the last 450 years. *Tectonics*, *38*(10), 3544–3562. https://doi.org/10.1029/2019TC005601

Suárez, G., García-Acosta, V., & Gaulon, R. (1994). Active crustal deformation in the Jalisco block, Mexico: Evidence for a great historical earthquake in the 16th century. *Tectonophysics*, *234*(1–2), 117–127. https://doi.org/10.1016/0040-1951(94)90207-0

Suárez, G., & Jaimes, M. A. (2023). Estimation of damage scenarios in Mexico City caused by nearby crustal earthquakes. *Bulletin of the Seismological Society of America*, *113*(1), 204–219. https://doi.org/10.1785/0120220186

Suárez, G., Ruiz-Barón, D., Chico-Hernández, C., & Zúñiga, F. R. (2020). Catalog of preinstrumental earthquakes in central Mexico: Epicentral and magnitude estimations based on macroseismic data. *Bulletin of the Seismological Society of America*, *110*(6), 3021–3036. https://doi.org/10.1785/0120200127

Sunye-Puchol, I., Lacan, P., Ortuño, M., Villamor, P., Audin, L., Zúñiga, F. R., et al. (2015). La Falla San Mateo: Nuevas evidencias paleosismológicas de fallamiento activo en el Graben de Acambay, México. *Revista Mexicana de Ciencias Geológicas*, *32*(3), 361–376.

Suter, M. (2008). Structural configuration of the Otates fault (southern Basin and Range Province) and its rupture in the 3 May 1887 MW 7.5 Sonora, Mexico, earthquake. *Bulletin of the Seismological Society of America*, *98*(6), 2879–2893. https://doi.org/10.1785/0120080129

Suter, M. (2015a). The A.D. 1567 M w 7.2 Ameca, Jalisco, earthquake (Western Trans-Mexican Volcanic Belt): Surface rupture parameters, seismogeological effects, and macroseismic intensities from historical sources. *Bulletin of the Seismological Society of America*, *105*(2A), 646–656. https://doi.org/10.1785/0120140163

Suter, M. (2015b). Rupture of the Pitáycachi fault in the 1887 M w 7.5 Sonora, Mexico earthquake (southern Basin-and-Range Province): Rupture kinematics and epicenter inferred from rupture branching patterns. *Journal of Geophysical Research: Solid Earth*, *120*(1), 617–641. https://doi.org/10.1002/2014JB011244

Suter, M. (2019). The 1563 MI 8 Puerto de la Navidad subduction-zone and 1567 Mw 7.2 Ameca crustal earthquakes (Western Mexico): New insights from sixteenth-century sources. *Seismological Research Letters*, *90*(1), 366–375. https://doi.org/10.1785/0220180304

Suter, M., Carrillo-Martínez, M., & Quintero-Legorreta, O. (1996). Macroseismic study of shallow earthquakes in the central and eastern parts of the Trans-Mexican Volcanic Belt, Mexico. *Bulletin of the Seismological Society of America*, *86*(6), 1952–1963.

Suter, M., Quintero, O., & Johnson, C. A. (1992). Active faults and state of stress in the central part of the Trans-Mexican Volcanic Belt, Mexico 1. The Venta de Bravo fault. *Journal of Geophysical Research*, *97*(B8), 11983. https://doi.org/10.1029/91JB00428

Suter, M., Quintero-Legorreta, O., López-Martínez, M., Aguirre-Díaz, G. J., & Farrar, E. (1995). The Acambay graben: Active intraarc extension in the Trans-Mexican Volcanic Belt, Mexico. *Tectonics*, *14*(5), 1245–1262. https://doi.org/10.1029/95tc01930

Szynkaruk, E., Garduño-Monroy, V. H., & Bocco, G. (2004). Active fault systems and tectono-topographic configuration of the central Trans-Mexican Volcanic Belt. *Geomorphology*, *61*(1–2), 111–126. https://doi.org/10.1016/j.geomorph.2003.10.006

Urbina, F., & Camacho, H. (1913). La zona megasísmica Acambay-Tixmadejé, Estado de México. *Boletín Instituto Geológico de México*, *32*, 1–125.

Wei, M., Sandwell, D., Fialko, Y., & Bilham, R. (2011). Slip on faults in the Imperial Valley triggered by the 4 April 2010 Mw 7.2 El Mayor-Cucapah earthquake revealed by InSAR. *Geophysical Research Letters*, *38*(1), n/a. https://doi.org/10.1029/2010GL045235

Wesnousky, S. G. (2008). Displacement and geometrical characteristics of earthquake surface ruptures: Issues and implications for seismic-hazard analysis and the process of earthquake rupture. *Bulletin of the Seismological Society of America*, *98*(4), 1609–1632. https://doi.org/10.1785/0120070111

Zúñiga, F. R., Lacan, P., Rodríguez-Pérez, Q., & Márquez-Ramírez, V. H. (2020). Temporal and spatial evolution of instrumented seismicity in the Trans-Mexican Volcanic Belt. *Journal of South American Earth Sciences*, *98*(February), 102390. https://doi.org/10.1016/j.jsames.2019.102390